Renormalized πNN coupling constant and the P-wave phase shifts in the cloudy bag model

B. C. Pearce and I. R. Afnan

School of Physical Sciences, The Flinders University of South Australia, Bedford Park, South Australia 5042, Australia
(Received 6 March 1986)

Most applications of the cloudy bag model to πN scattering involve unitarizing the bare diagrams arising from the Lagrangian by iterating in a Lippmann-Schwinger equation. However, analyses of the renormalization of the coupling constant proceed by iterating the Lagrangian to a given order in the bare coupling constant. These two different approaches means there is an inconsistency between the calculation of phase shifts and the calculation of renormalization. A remedy to this problem is presented that has the added advantage of improving the fit to the phase shifts in the P_{11} channel. This is achieved by using physical values of the coupling constant in the crossed diagram which reduces the repulsion rather than adds attraction. This approach can be justified by examining equations for the $\pi\pi$N system that incorporate three-body unitarity.

I. INTRODUCTION

Chiral bag models have enjoyed a considerable degree of popularity in recent years, due to their ability to incorporate quark degrees of freedom in descriptions of meson-baryon interactions. In particular, the version known as the cloudy bag model (CBM) has been used with apparent success in both the πN (Refs. 1–3) and KN (Ref. 4) sectors. However, despite the initial success in describing the low energy P_{33} πN phase shifts, most attempts in the P_{11} channel[3,5] have been disappointed to say the least. The P_{11} phase shifts have traditionally been difficult to describe, requiring a detailed cancellation between the low energy repulsion from the nucleon pole and the attractive mechanisms that dominate at higher energies to produce the Roper resonance. Calculations based on iterating the basic CBM interactions in a Lippmann-Schwinger equation have usually produced an amplitude that is much too repulsive at low energies, a consequence of relying on a Roper pole term to provide the dominant attraction. Although this is quite capable of forcing the phase shifts through 90° at the Roper resonance energy, it does not provide enough attraction at low energy to cancel the repulsion and produce the small, negative phase shifts.

It is clear from the large probability for decay of the Roper resonance via the process $R \rightarrow \pi\Delta \rightarrow \pi\pi N$ that a complete description of the P_{11} channel in the vicinity of the Roper resonance should include contributions from at least two pion states which are omitted in the usual Lippmann-Schwinger approach. This is evident in purely phenomenological calculations which, although reproducing the phase shifts quite well, are incapable of becoming inelastic below the $\pi\Delta$ threshold.[6] Although ideally these contributions would be included in a three-body description, an improvement to the fit in the P_{11} channel has been obtained by phenomenological inclusion of a $\pi\pi$ interaction into a CBM description.[7]

The above calculations all generate unitary phase shifts by iterating the elementary diagrams that arise from the CBM Lagrangian in a Lippmann-Schwinger equation. This procedure gives rise to a renormalization of the bare

πNN coupling constant, which can be determined from the residue of the πN amplitude at the nucleon pole. However, to date, the only estimation of the effects of renormalization on the coupling constant have relied on the calculation of a small subset of diagrams from the multiple scattering series.[2] This indicated that the renormalization was small, with a bare coupling constant squared of about 0.09–0.10 needed to reproduce the experimental value of 0.08. Consequently, all of the analyses of πN scattering described above have used bare coupling constants in this range. In this paper we examine the implications of removing this discrepancy between the calculation of phase shifts, and the calculation of the renormalization, by extracting the value of the renormalized coupling constant directly from the Lippmann-Schwinger equation. The results of this are somewhat disturbing. We find that if we use the bare coupling constant suggested, then the renormalized coupling constant squared turns out to be too small (about 0.06). Closer examination shows that the discrepancy arises because some diagrams important to the calculation of the renormalization are not included in the partial summation of the perturbation series via the Lippmann-Schwinger equation. These diagrams are excluded from the Lippman-Schwinger equation, which only respects two-body unitarity, but are partly included in a description of πN scattering that satisfies two and three-body unitarity. This observation leads us to examine the consequences of starting with equations that obey two- and three-body unitarity and then neglecting contributions which are unimportant at low energies. What we find is that the bare coupling constant should only appear in the pole diagram. The vertices that form the crossed diagram are dressed and therefore should have the experimental coupling constant. This significantly reduces the magnitude of the bare coupling constant required to reproduce the physical value. As a result, the strength of the repulsive nucleon pole diagram is reduced while the attractive crossed and contact diagrams remain approximately the same, resulting in an immense improvement in the P_{11} phase shifts.

The equations we present in this paper are general,

needing as their input B↔πB and πB↔πB interactions. These interactions can be taken either from a microscopic description such as a bag model or phenomenology. In this paper we use the version of the CBM in which the

pions couple to the quarks throughout the bag volume.[8] After expansion to second order in the pion field ϕ the Lagrangian is

$$\mathcal{L} = \left[\frac{i}{2}\bar{q}(x)\gamma^\mu \overleftrightarrow{\partial}_\mu q(x) - B \right]\theta_V - \frac{1}{2}\bar{q}(x)q(x)\Delta_S + \frac{1}{2}(\partial_\mu\phi)^2 + \frac{1}{2f_\pi}\bar{q}(x)\gamma^\mu\gamma_5\tau\cdot\partial_\mu\phi q(x)\theta_V - \frac{1}{4f_\pi^2}\bar{q}(x)\gamma^\mu\tau\cdot(\phi\times\partial_\mu\phi)q(x)\theta_V \ ,$$

(1.1)

where $q(x)$ and $\phi(x)$ are the quark and pion fields, f_π is the pion decay constant, and B is the bag energy density. Δ_S is a surface delta function and θ_V is 1 inside and 0 outside the bag. After projection onto the baryon subspace (see Appendix), the interaction part of this Lagrangian contains a B↔πB vertex [see Fig. 1(a)], a πB↔πB contact term [Fig. 1(b)], as well as a B↔ππB vertex [Fig. 1(c)] which is not included in the present analysis.

In Sec. II we show how to extract the renormalized coupling constant from the Lippmann-Schwinger equation, including a discussion of how to correctly handle the inclusion of N* states. The results of this procedure are presented in Sec. III. Section IV summarizes the three-body ππN equations which have been formulated in Ref. 9 and shows the implications to the purely two-body system with the results presented in Sec. V. In Sec. VI we present our conclusions. The CBM Lagrangian and the basic diagrams that arise after projection onto the baryon subspace and form the input to our equations are described in detail in the Appendix.

II. TWO-BODY EQUATIONS: FORMALISM

In this section we show how the coupling constant and mass renormalizations are calculated to the same order as is obtained by solving the Lippmann-Schwinger equation. The method is to reorganize the diagrams summed by the Lippmann-Schwinger equation into pole and nonpole parts and then extract the coupling constant from the pole part. This can be done either by direct manipulation of the Lippmann-Schwinger equation with a potential consisting of a pole and nonpole terms,[10,11] or by the technique of classification of diagrams according to their irreducibility.[12] The latter method has been applied to the πB system in Ref. 13 and we merely summarize the results here.

Before we can classify the set of all diagrams contributing to the process πB↔πB (B=nucleon or delta), propagator dressing must be carried out on all baryons in order to ensure that all cuts that separate initial and final states lead to connected diagrams.[13] We implement this, in practice, by ensuring that internal πB propagators use the

physical baryon masses and by associating a factor of $Z_2^{1/2}$ with each external baryon leg (Z_2 is the baryon wave function renormalization constant). In so doing, we are assuming that the factor of Z_2 which arises from dressing a baryon line in the presence of another pion can be neglected. This assumption, which also avoids self-consistency problems in calculating Z_2, will be reconsidered in Sec. IV.

Using the technique of classification of diagrams, the amplitude for πB scattering $t^{(0)}$ can be expressed as the sum of a pole and nonpole[13] terms

$$t^{(0)}(E) = t^{(1)}(E) + f^{(1)\dagger}(E)d(E)f^{(1)}(E) \ ,$$

(2.1)

where t is the πB↔πB amplitude, f is the B←πB amplitude, and d is the dressed B propagator. The superscript refers to the irreducibility of the amplitude.[12] The nucleon and delta are treated on the same footing in the sense that t is 2×2 matrix. If the Roper pole is to be included, then f is a 3×2 matrix and d is 3×3. If the Roper is excluded, then f and d are both 2×2 matrices. The nonpole part of the amplitude, $t^{(1)}$, satisfies a Lippmann-Schwinger equation with driving potential $t^{(2)}$,

$$t^{(1)}(E) = t^{(2)}(E) + t^{(2)}(E)g(E)t^{(1)}(E) \ ,$$

(2.2)

where g is the one particle irreducible πB propagator. Here, $f^{(1)}$ is written in terms of the two-particle irreducible B←πB vertex $f^{(2)}$ as

$$f^{(1)}(E) = f^{(2)} + f^{(2)}g(E)t^{(1)}(E) \ .$$

(2.3)

The dressed baryon propagator appearing in Eq. (2.1) is given by

$$d^{-1}(E) = d^{(0)-1}(E) - \Sigma^{(1)}(E) \ ,$$

(2.4)

where the self-energy $\Sigma^{(1)}(E)$ is given by

$$\Sigma^{(1)}(E) = f^{(1)}(E)g(E)f^{(2)\dagger}$$

(2.5)

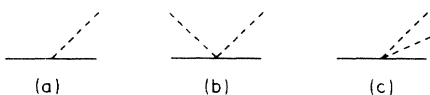and the bare baryon propagator $d^{(0)}$ is a diagonal matrix with elements

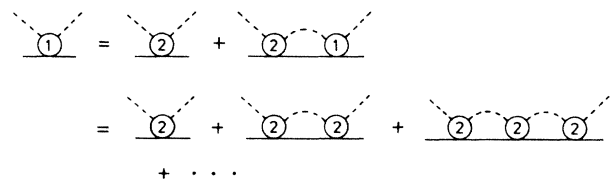FIG. 1. Diagrammatic content of the CBM Lagrangian. (a) B←πB vertex, (b) πB↔πB contact term, and (c) B←ππB vertex.

FIG. 2. The nonpole amplitude $t^{(1)}$.

$$d_\alpha^{(0)-1}(E)=E-m_\alpha^{(0)} ,\qquad (2.6)$$

where $m_\alpha^{(0)}$ is the bare mass of baryon α.

If we are concerned with maintaining only two-body unitarity, then the vertex $f^{(2)}$ and the amplitude $t^{(2)}$ can be taken from phenomenology or a bag model. With this choice the diagrammatic content of Eqs. (2.2), (2.3), and (2.5) are illustrated in Figs. 2, 3, and 4 respectively. We also take the πB propagator g to be real and diagonal with poles appropriate to physical masses. That is, we take

$$g_\alpha(p;E)=[E-(p^2+m_\alpha^2)^{1/2}-(p^2+m_\pi^2)^{1/2}]^{-1} .\qquad (2.7)$$

It should be noted that Eqs. (2.1)–(2.6) are equivalent to solving the Lippmann-Schwinger equation[10,11]

$$t^{(0)}(E)=v(E)=v(E)g(E)t^{(0)}(E)\qquad (2.8)$$

with the potential

$$v(E)=t^{(2)}(E)+f^{(2)\dagger}d^{(0)}(E)f^{(2)} .\qquad (2.9)$$

Before Eqs. (2.1)–(2.6) can be used, it is necessary to perform a partial wave expansion in order to reduce the dimensionality of the integrals. After partial wave expansion and consideration of the matrix nature of the equations, the $\pi B \leftrightarrow \pi B$ amplitude is labeled by the orbital angular momentum (l), the total angular momentum (J), and the total isospin (T), as well as the initial and final baryons (α, β, γ, etc.). The baryon labels run over the nucleon and delta as well as the Roper where appropriate. Equation (2.1) becomes

$$t_{\alpha\beta}^{(0)lJT}(p_\alpha,p_\beta;E)=t_{\alpha\beta}^{(1)lJT}(p_\alpha,p_\beta;E)$$
$$+\sum_{\gamma\eta\in\{lJT\}}f_{\pi\alpha\gamma}^{(1)}(p_\alpha;E)d_{\gamma\eta}^{lJT}(E)$$
$$\times f_{\eta\beta\pi}^{(1)}(p_\beta;E) ,\qquad (2.10)$$

where the sum is over all baryons with quantum numbers (lJT) (e.g., nucleon and Roper when $lJT\equiv P_{11}$). The nonpole part, Eq. (2.2), becomes

$$t_{\alpha\beta}^{(1)lJT}(p_\alpha,p_\beta;E)=t_{\alpha\beta}^{(2)lJT}(p_\alpha,p_\beta;E)$$
$$+\sum_\gamma\int_0^\infty dp_\gamma p_\gamma^2 t_{\alpha\gamma}^{(2)lJT}(p_\alpha,p_\gamma;E)$$
$$\times g_\gamma(p_\gamma;E)t_{\gamma\beta}^{(1)lJT}(p_\gamma,p_\beta;E) .$$
$$(2.11)$$

Since the $B\leftrightarrow\pi B$ amplitude only has a contribution from $l=1$, the only labels required are the initial and final baryons. We also write $f_{\alpha\beta\pi}$ and $f_{\pi\alpha\beta}$ in place of $f_{\alpha\beta}$ and $f_{\alpha\beta}^\dagger$, respectively, to obtain
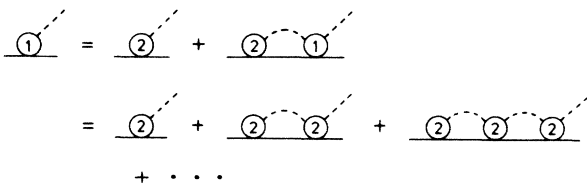

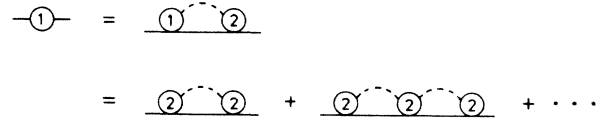FIG. 3. The dressed πNN vertex $f^{(1)}$.

FIG. 4. The self-energy $\Sigma^{(1)}$.

$$f_{\alpha\beta\pi}^{(1)}(p_\beta;E)=f_{\alpha\beta\pi}^{(2)}(p_\beta)+\sum_\gamma\int_0^\infty dp_\gamma p_\gamma^2 f_{\alpha\gamma\pi}^{(2)}(p_\gamma)g_\gamma(p_\gamma;E)$$
$$\times t_{\gamma\beta}^{(1)\alpha}(p_\gamma,p_\beta;E) .\qquad (2.12)$$

The superscript α is used to denote that the nonpole amplitude $t^{(1)}$ is projected onto the partial wave whose quantum numbers (lJT) match those of the baryon α. Note that this amplitude is the same for $\alpha=N$ and $\alpha=R$. Finally, Eqs. (2.4) and (2.5) become

$$d_{\alpha\beta}^{lJT-1}(E)=\delta_{\alpha\beta}d_\alpha^{(0)-1}(E)-\Sigma_{\alpha\beta}^{lJT}(E)\qquad (2.13)$$

and

$$\Sigma_{\alpha\beta}^{(1)lJT}(E)=\sum_\gamma\int_0^\infty dp_\gamma p_\gamma^2 f_{\alpha\gamma\pi}^{(1)}(p_\gamma;E)$$
$$\times g_\gamma(p_\gamma;E)f_{\pi\gamma\beta}^{(2)}(p_\gamma) ,\qquad (2.14)$$

where $(\alpha,\beta)\in\{lJT\}$.

In order to extract the renormalized coupling constant from the pole part of Eq. (2.1), we must ensure that $d^{P_{11}}(E)$ has a pole with residue one at the nucleon mass. If there were only one baryon associated with each partial wave (which would be the case if the Roper were omitted), then this can be done quite simply. The technique is essentially the same as in Ref. 14, except that here we are dealing with matrices. The situation is more difficult if the Roper is to be included since the dressed baryon propagator $d(E)$ is not diagonal. In the P_{11} channel it is (dropping the lJT superscript)

$$d^{-1}(E)=\begin{bmatrix} E-m_N^{(0)}-\Sigma_{NN}^{(1)}(E) & -\Sigma_{NR}^{(1)}(E) \\ -\Sigma_{RN}^{(1)}(E) & E-m_R^{(0)}-\Sigma_{RR}^{(1)}(E) \end{bmatrix} .$$
$$(2.15)$$

Since this matrix is real-symmetric for $E<m_N+m_\pi$, it can be diagonalized by an orthogonal matrix U such that

$$\tilde{d}(E)\equiv U^T d(E)U$$

$$=\begin{bmatrix} E-m_N^{(0)}-\tilde{\Sigma}_N(E) & 0 \\ 0 & E-m_R^{(0)}-\tilde{\Sigma}_R(E) \end{bmatrix}^{-1}\qquad (2.16)$$

with

$$\tilde{\Sigma}_N(E)=\tfrac{1}{2}(m_R^{(0)}-m_N^{(0)}+\Sigma_{NN}^{(1)}(E)+\Sigma_{RR}^{(1)}(E)$$
$$-\{[m_R^{(0)}+\Sigma_{RR}^{(1)}(E)-m_N^{(0)}-\Sigma_{NN}^{(1)}(E)]^2$$
$$+4\Sigma_{NR}^{(1)2}(E)\}^{1/2})\qquad (2.17)$$

and

$$\widetilde{\Sigma}_R(E) = \tfrac{1}{2}(m_N^{(0)} - m_R^{(0)} + \Sigma_{NN}^{(1)}(E) + \Sigma_{RR}^{(1)}(E)$$
$$+ \{[m_R^{(0)} + \Sigma_{RR}^{(1)}(E) - m_N^{(0)} - \Sigma_{NN}^{(1)}(E)]^2$$
$$+ 4\Sigma_{NR}^{(1)^2}(E)\}^{1/2}) . \qquad (2.18)$$

The orthogonal matrix U is given by

$$U = \frac{1}{(1+v^2)^{1/2}} \begin{bmatrix} 1 & v \\ -v & 1 \end{bmatrix} \qquad (2.19)$$

with

$$v = \frac{\Sigma_{NN}^{(1)}(E) - \widetilde{\Sigma}_N(E)}{\Sigma_{NR}^{(1)}(E)} = \frac{\widetilde{\Sigma}_R(E) - \Sigma_{RR}^{(1)}(E)}{\Sigma_{NR}^{(1)}(E)} . \qquad (2.20)$$

Defining

$$\widetilde{f}_{\alpha\beta\pi}^{(1)}(p;E) \equiv \sum_{\gamma=N,R} U_{\alpha\gamma} f_{\gamma\beta\pi}^{(1)}(p;E) \quad (\alpha=N,R;\ \beta=N,\Delta) , \qquad (2.21)$$

with a similar expression for $\widetilde{f}_{\pi\alpha\beta}^{(1)}$, enables us to write Eq. (2.10) as (neglecting the IJT superscript since we are only considering the P_{11} channel here)

$$t_{\alpha\beta}^{(0)}(p_\alpha, p_\beta; E) = t_{\alpha\beta}^{(1)}(p_\alpha, p_\beta; E)$$
$$+ \sum_{\gamma=N,R} \widetilde{f}_{\pi\alpha\gamma}^{(1)}(p_\alpha; E) \widetilde{d}_\gamma(E) \widetilde{f}_{\gamma\beta\pi}^{(1)}(p_\beta; E) . \qquad (2.22)$$

This procedure ensures that we are correctly treating the physical nucleon as an admixture of bare nucleon $[(1s_{1/2})^3]$ and Roper $[(1s_{1/2})^2(2s_{1/2})]$ bag states. Typically, we find that U_{NR} is about 10% of U_{NN}.

Now that we have diagonalized the dressed baryon propagator, the procedure for extracting the renormalized coupling constant is straightforward. First, we expand $\widetilde{\Sigma}_N(E)$ in a Taylor series about m_N to write

$$\widetilde{\Sigma}_N(E) = \widetilde{\Sigma}_N(m_N) + (E - m_N)\widetilde{\Sigma}_{1N} + (E - m_N)^2 \widetilde{\Sigma}_{2N}(E) , \qquad (2.23)$$

where

$$\widetilde{\Sigma}_{1N} = \frac{\partial}{\partial E} \widetilde{\Sigma}_N \bigg|_{E=m_N} , \qquad (2.24)$$

and $\widetilde{\Sigma}_{2N}(E)$ is a function chosen to produce the equality. If we choose the nucleon bare mass such that

$$m_N = m_N^{(0)} + \widetilde{\Sigma}_N(m_N) , \qquad (2.25)$$

then from Eq. (2.16) we have

$$\widetilde{d}_N^{-1}(E) = (E - m_N)(1 - \widetilde{\Sigma}_{1N}) \left[1 - \frac{(E - m_N)\widetilde{\Sigma}_{2N}(E)}{1 - \widetilde{\Sigma}_{1N}} \right] , \qquad (2.26)$$

or

$$\widetilde{d}_N(E) = \widetilde{d}_N^R(E) Z_{2N} , \qquad (2.27)$$

where the nucleon wave function renormalization constant is

$$Z_{2N} = (1 - \widetilde{\Sigma}_{1N})^{-1} \qquad (2.28)$$

and the renormalized nucleon propagator is

$$\widetilde{d}_N^R(E) = (E - m_N)^{-1}[1 - (E - m_N)Z_{2N}\widetilde{\Sigma}_{2N}(E)]^{-1} . \qquad (2.29)$$

Note that $\widetilde{d}_N^R(E)$ has the desired property of a pole at $E = m_N$ with residue one. It is now a simple matter to extract the renormalized coupling constant from Eq. (2.22) by evaluating the pole part at $E = m_N$, giving us

$$f_{\pi NN}^R = f_{\pi NN} \frac{\widetilde{f}_{\pi NN}^{(1)}(p_0, m_N)}{f_{\pi NN}^{(2)}(p_0)} Z_{2N} u(p_0 R) , \qquad (2.30)$$

where p_0 is the on-shell momentum. $u(p_0 R)$ is the bag vertex function given in Eq. (A4) and is necessary for comparison with the Feynman diagrams in terms of which the experimental coupling constant is defined. The factor of Z_{2N} arises as a consequence of the baryon dressing discussed at the beginning of Sec. II and $f_{\pi NN}$ is the bare coupling constant appearing in Eq. (A2). If the Roper pole term is to be omitted, then we replace $\widetilde{f}^{(1)}$ by $f^{(1)}$ in Eq. (2.30) and $\widetilde{\Sigma}_N$ by $\Sigma_{NN}^{(1)}$ in Eq. (2.24).

If Eqs. (2.3) and (2.5) are truncated to the first two and the first terms in their series expansions, respectively (see Figs. 3 and 4), if the Roper pole diagram is omitted, and if the two-particle irreducible amplitude $t^{(2)}$ is taken to be the crossed diagram, then Eq. (2.30) is the same prescription as that used by Theberge, Miller, and Thomas.[2] The factor of $\widetilde{f}_{\pi NN}^{(1)}(p_0, m_N)/f_{\pi NN}^{(2)}(p_0)$ is equivalent to Z_1^{-1} in their notation.

III. TWO-BODY EQUATIONS: RESULTS

We can now begin to examine the consequences of the above approach to renormalization. If the Roper and the contact diagram are excluded and the series expansions are truncated as described above, then we have the same model as Ref. 2, except that we use relativistic πB propagators and include baryon recoil in the crossed diagram. The bare coupling constant $f_{\pi NN}$ is adjusted so that $f_{\pi NN}^R$ defined above is the experimental value of $\sqrt{0.08}$. The bare delta mass only enters into the P_{33} channel and therefore does not affect the determination of the bare coupling constant. Its value can be determined by the requirement that the P_{33} phase shift go through 90° at the delta mass. Since the bare nucleon mass is determined from Eq. (2.25), the only undetermined parameter is the bag radius. The difference between truncating the series as in Ref. 2 (solid curve) and using the full series (dashed curve) can be seen in Fig. 5, which shows the bare coupling constant $f_{\pi NN}^2$, the nucleon wave function renormalization Z_{2N}, and the bare nucleon mass as functions of the bag radius. It is clear from these graphs that including the higher terms in the series (generated by the Lippmann-Schwinger equation) dramatically alters the renormalization results. Closer examination shows that most of the difference comes from the second term in the series for $\Sigma^{(1)}$ (omitted in Ref. 2) which has a contribution of about 50% of the first term for a bag radius of 1 fm. Also, for radii less than 1 fm, using the full series expan-
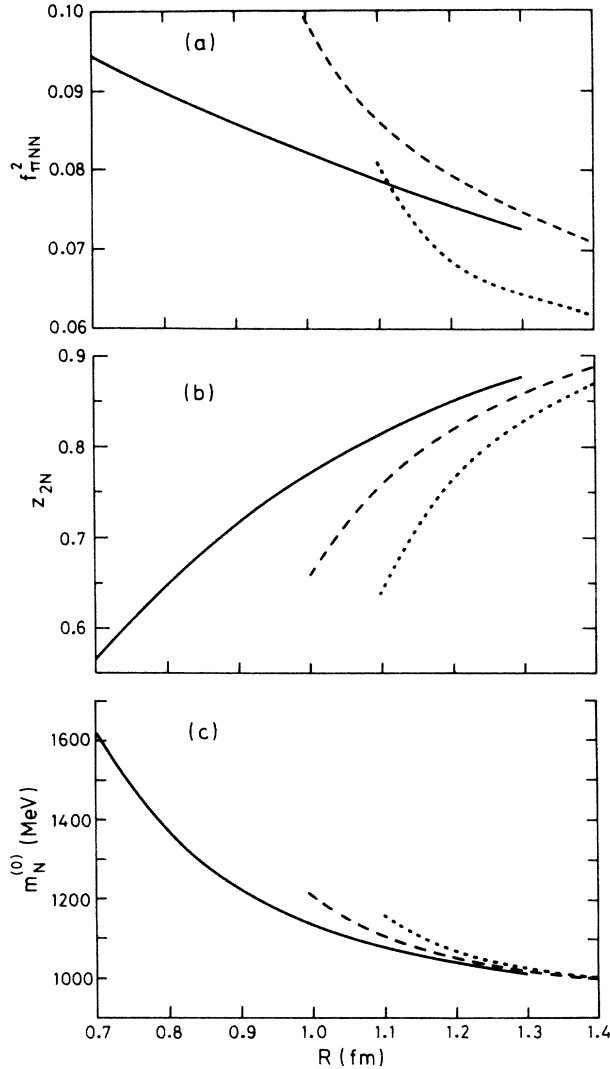
FIG. 5. The bare coupling constant, nucleon wave function renormalization, and bare nucleon mass as functions of the bag radius. The solid curve is with the truncation described in the text, the dashed curve is without truncation, and the dotted curve is without truncation and including the contact diagram.

sions, there is no bare coupling constant that will reproduce the experimental value. This is reflected in the fact that the wave function renormalization constant, Z_{2N}, becomes alarmingly small. Since Z_{2N} is the probability of finding a bare bag, it indicates that, for radii less than about 1 fm, pionic effects are very important and the nucleon is essentially a πN bound state.

The effect of including the contact diagram is to decrease the required bare coupling constant, as can be seen in Fig. 5 (dotted curve). Apart from this minor difference, its inclusion does not alter the basic results.

An explanation of these undesirable features can be found by a careful examination of the diagrams that have been included and those that have been excluded. In Figs. 6 and 7 we show all contributions in perturbation theory to the vertex and the derivative of the self-energy to fifth and fourth order, respectively, in the bare coupling constant. In Fig. 7 the $\times$ indicates which propagator the
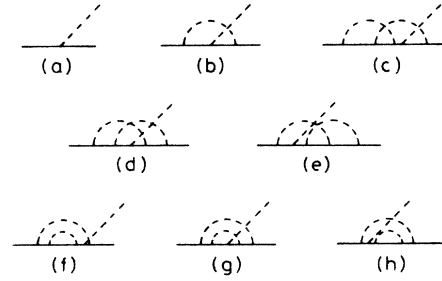

FIG. 6. All contributions to the vertex function up to fifth order in the coupling constant in a model with only a vertex interaction.

derivative acts on. It can be seen that there is a one to one correspondence between diagrams of each series. Note that Figs. 6(a)—(6c) and 7(a)—7(d) are explicitly included in the expansions of Eqs. (2.3) and (2.5), while Figs. 6(f), 6(h), 7(e), and 7(g) are included implicitly since the πB propagators have the physical baryon masses. Since the degree of normalization is essentially the ratio of the terms in these two figures [see Eqs. (2.30) and (2.28)], it is important that for each diagram included in $f^{(1)}$ the corresponding diagram be included in $(\partial/\partial E)\Sigma^{(1)}$ and vice versa. However, Figs. 6(d) and 6(e) are not included in our expansion of $f^{(1)}$, but their corresponding diagrams [Figs. 7(c) and 7(d)] are included in $(\partial/\partial E)\Sigma^{(1)}$. A rough estimation suggests that the contribution from Figs. 6(d) and 6(e) should be similar in magnitude to that of Fig. 6(c) and hence should be included. To put this into perspective, for a bag radius of 1 fm and $f^2_{\pi NN}=0.08$, the contribution of Fig. 6(c) is about 10% of the sum of Figs. 6(a) and 6(b). Similar diagrams are omitted from $f^{(1)}$ at higher order in the coupling constant, while their counterparts are included in $(\partial/\partial E)\Sigma^{(1)}$.

From this discussion it can be seen that the essence of the problem is that the Lippmann-Schwinger equation omits a certain class of diagrams which play a crucial role in the calculation of the coupling constant. It may be that, due to the correspondence between diagrams contributing to $f^{(1)}$ and those contributing to $(\partial/\partial E)\Sigma^{(1)}$, the truncation to Figs. 6(a), 6(b), and 7(a) (as in Ref. 2) will yield something close to the correct result. However, if
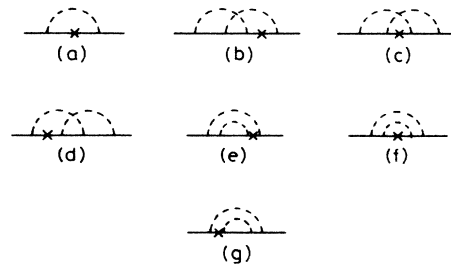

FIG. 7. All contributions to the derivative of the self-energy up to fourth order in the coupling constant in a model with only a vertex interaction. The cross indicates which propagator the derivative acts on.

one then uses the resulting bare coupling constant to define the crossed and pole diagrams and iterates them in a Lippmann-Schwinger equation to calculate the phase shifts, then our results show that the physical coupling constant embedded in the calculation of the phase shifts will not be the experimental value of 0.08. In fact, using the same parameters as used in Ref. 3 to compute the P_{11} phase shifts ($R = 1$ fm, $f_{\pi NN}^2 = 0.074$, $m_R^{(0)} = 1510$ MeV, and $f_\pi = 97$ MeV), the renormalized coupling constant squared turns out to be 0.064.

A clue to a means of remedying this situation can be found by observing that the Lippmann-Schwinger equation is guaranteed to respect only up to two-body unitarity, while Figs. 6(d) and 6(e) are excluded because they only contribute to three-body unitarity. This leads us to the next section, where we examine the consequences to renormalization of including three-body unitarity in the πB equations.

IV. THREE-BODY EQUATIONS: FORMALISM

In Eqs. (2.1)–(2.6), we present a description of πB scattering that guarantees at least two-body unitarity. Although they can be derived directly from the Lippmann-Schwinger equation, their derivation in terms of classification of diagrams according to their reducibility makes it relatively straightforward to include three-body unitarity. This has been done in Ref. 9, and we simply summarize the results here. The technique is to expose three-particle unitarity cuts for all quantities that are two-particle irreducible (particularly $t^{(2)}$) using the last cut lemma. This will produce amplitudes that are three-particle irreducible and provide a connection to the $\pi\pi$B Hilbert space.

In the two-body equations used above, the only interactions that are needed from the interaction Lagrangian are those whose initial and final states are from the one- and two-body Hilbert spaces. Including the three-body Hilbert space means that the B$\leftarrow\pi\pi$B diagram of order f_π^{-2}, shown in Fig. 1(c), which provides a direct connection between the one- and three-body Hilbert spaces, now needs to be considered. Unfortunately, inclusion of this term tends to make the resulting equations somewhat unwieldly. For the time being we shall restrict our basic interactions to the B$\leftarrow\pi$B vertex and direct πB$\leftrightarrow\pi$B interactions such as the contact diagram.

Previously, the only two-body initial and final states were πB states. Now we have the possibility of πB*, where B* is a πB resonance, and ρB, where ρ is a $\pi\pi$ resonance. As a consequence, we need to modify our notation. We refer to the two pions as particles 1 and 2 and the baryon as particle 3. For $\lambda = 1$ or 2, $T_{\lambda B}$ will denote an amplitude with πB* final state, where B* is a bound state of pion λ and the baryon, while T_{3B} represents an amplitude with a ρB final state. Since the amplitude for πB$\leftrightarrow\pi$B couples to $T_{\lambda B}$, for consistency we use T_{BB} in place of t. We retain the superscripts referring to the irreducibility of the amplitude and drop the energy argument, which is understood. The nucleon and delta are still treated on an equal footing through the matrix nature of the amplitudes. Using this notation, Eqs. (2.1) and (2.3) become

$$T_{BB}^{(0)} = T_{BB}^{(1)} + f^{(1)\dagger} d f^{(1)} \tag{4.1}$$

and

$$f^{(1)} = f^{(2)}(1 + g T_{BB}^{(1)}), \tag{4.2}$$

while Eqs. (2.4) and (2.5) are unchanged. $T_{BB}^{(1)}$ is a solution of the coupled set of equations

$$T_{BB}^{(1)} = \left[t^{(3)} + \sum_{ij} F_d^{(2)}(i) G \bar{\delta}_{ij} F_d^{(2)\dagger}(j) \right] (1 + g T_{BB}^{(1)})$$
$$+ \sum_{i\alpha} F_d^{(2)}(i) G \bar{\delta}_{i\alpha} M_d^{(2)}(\alpha) G T_{\alpha B}^{(1)} \tag{4.3a}$$

and

$$T_{\lambda B}^{(1)} = \sum_i \bar{\delta}_{\lambda i} F_d^{(2)\dagger}(i)(1 + g T_{BB}^{(1)})$$
$$+ \sum_\alpha \bar{\delta}_{\lambda\alpha} M_d^{(2)}(\alpha) G T_{\alpha B}^{(1)}. \tag{4.3b}$$

Here, F is used to denote a πB$\leftarrow\pi\pi$B amplitude, while M describes the process $\pi\pi$B$\leftrightarrow\pi\pi$B. The subscript d means that the amplitude is the disconnected part only. Throughout this section, a number in parentheses following an amplitude indicates which pion takes part in the interaction, with the exception of the $\pi\pi$B$\leftrightarrow\pi\pi$B amplitude M_d. In this case, if the number is a 1 or 2 it refers to the pion taking part in the interaction, while a 3 labels the amplitude in which the baryon is a spectator. The Latin letters i, j, etc. are used where the sum is over the two pions and Greek letters indicate summation over the pions and baryon. Also, $\bar{\delta}_{\alpha\beta} = 1 - \delta_{\alpha\beta}$. Note that the contact diagram of Fig. 1(b) now enters through the three-particle irreducible amplitude $t^{(3)}$. The above equations are similar to those presented by Fuda[15] for the $\pi\pi$N sytsem using projection operator techniques. The amplitudes $F_d^{(2)}$ and $M_d^{(2)}$ can be written as

$$F_d^{(2)}(i) = \sum_j d_\pi^{-1}(j) f^{(1)}(i) \bar{\delta}_{ij} \tag{4.4}$$

and

$$M_d^{(2)}(\alpha) = \begin{cases} \sum_i d_\pi^{-1}(i) T_{BB}^{(1)}(\alpha) \bar{\delta}_{i\alpha} & \text{if } \alpha = 1, 2, \\ d^{-1} t^{(1)}(3) & \text{if } \alpha = 3. \end{cases} \tag{4.5}$$

In the above, $d_\pi(i)$ is the propagator of pion i, d is the baryon propagator, and $t^{(1)}(3)$ is the one-particle irreducible $\pi\pi\leftrightarrow\pi\pi$ amplitude. Note that the 2×2 matrix structure of M_d^2 is maintained since d_π and $t^{(1)}(3)$ are scalars, while $T_{BB}^{(1)}(i)$ and d are matrices. The center of mass (c.m.) energy ϵ at which the amplitudes $T_{BB}^{(1)}(i)$ and $f^{(1)}$ appearing in Eqs. (4.4) and (4.5) are needed will always satisfy $\epsilon = E - \omega_p < E - m_\pi$, where E is the c.m. energy at which the πB$\leftrightarrow\pi$B amplitude $T_{BB}^{(0)}$ of Eq. (4.1) is required. Hence it is always possible to work up in energy from below the scattering threshold, where $T_{BB}^{(1)}$ and therefore $f^{(1)}$ are real in Eqs. (4.4) and (4.5), and the coupling to the πB* and ρB can be neglected.

Equations (4.4) and (4.5) are expressed diagrammatically in Figs. 8 and 9, respectively. Note that the crossed di-

agram arises in Eq. (4.3a) from the term

$$\sum_{ij} F_d^{(2)}(i)G\bar{\delta}_{ij}F_d^{(2)\dagger}(j)=\sum_{ij} f^{(1)}(i)d\bar{\delta}_{ij}f^{(1)\dagger}(j) \ . \qquad (4.6)$$

An important feature of this is that the vertices that form this diagram are dressed.

In order to examine the diagrammatic content of these equations, substitute Eq. (4.3a) into Eq. (4.2) to give (for

FIG. 8. The disconnected πB$\leftarrow\pi\pi$B amplitude $F_d^{(2)}$.

the purposes of this discussion we neglect the contact diagram $t^{(3)}$)

$$f^{(1)}=f^{(2)}+f^{(2)}g\sum_{ij} F_d^{(2)}(i)G\bar{\delta}_{ij}F_d^{(2)\dagger}(j)(1+gT_{BB}^{(1)})+f^{(2)}g\sum_{i\alpha} F_d^{(2)}(i)G\bar{\delta}_{i\alpha}M_d^{(2)}(\alpha)GT_{\alpha B}^{(1)} \ . \qquad (4.7)$$

Iterating Eq. (4.3) to lowest order and substituting into Eq. (4.7) gives

$$f^{(1)}=f^{(2)}+f^{(2)}g\sum_{ij} F_d^{(2)}(i)G\bar{\delta}_{ij}F_d^{(2)\dagger}(j)+f^{(2)}g\sum_{ij} F_d^{(2)}(i)G\bar{\delta}_{ij}F_d^{(2)\dagger}(j)g\sum_{kl} F_d^{(2)}(k)G\bar{\delta}_{kl}F_d^{(2)\dagger}(l)$$

$$+f^{(2)}g\sum_{i\alpha} F_d^{(2)}(i)G\bar{\delta}_{i\alpha}M_d^{(2)}(\alpha)G\sum_j \bar{\delta}_{\alpha j}F_d^{(2)\dagger}(j)+ \cdots \ . \qquad (4.8)$$

Figure 10 shows the content of this equation, which should be compared with Fig. 6, which shows all diagrams arising in perturbation theory (from a Lagrangian in which there is only a B$\leftarrow\pi$B interaction) to fifth order in the coupling constant. If all propagators include the baryon dressing (i.e., have poles corresponding to physical masses), then Eq. (4.8) includes all diagrams arising from the perturbation expansion. In particular, Figs. 6(b), 6(e), and 6(g) are contained in the second term of Eq. (4.8), Fig. 6(c) is contained in the third term, while Fig. 6(d) arises from the fourth term. Figures 6(f) and 6(h) are also contained in the second term of Eq. (4.8) by virtue of the baryon dressing.

Our main reason for introducing three-body unitarity at this stage was to shed some light on the problem discussed in Sec. III. There it was found that iterating a potential consisting of a pole and crossed diagram constructed from the bare vertices of the Lagrangian gives an inconsistent result due to the exclusion of some diagrams for the Lippmann-Schwinger equation that are important in the context of renormalization. As we have just seen, these diagrams are included in the three-body equations. The three-body equations clearly include dynamical processes not present in a two-body description that will be important above the pion production threshold, namely the formation and decay of πB* and ρB states described by $T_{\lambda B}^{(1)}$. However, for low energy scattering processes these effects will be small and can be neglected. This will decouple Eqs. (4.3), giving us

$$T_{BB}^{(1)}=\left[t^{(3)}+\sum_{ij} F_d^{(2)}(i)G\bar{\delta}_{ij}F_d^{(2)\dagger}(j)\right](1+gT_{BB}^{(1)}) \ . \qquad (4.9)$$

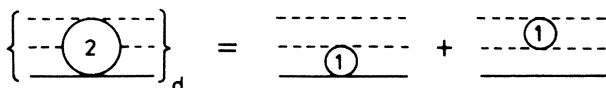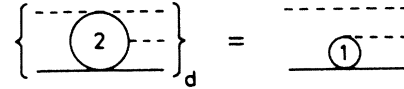The only difference between this and the approach outlined in Sec. II is that now the vertices appearing in the

crossed diagram are dressed and have an energy dependence. The solution of Eqs. (4.2) and (4.9) involves an apparent self-consistency, to the extent that Eq. (4.2) gives $f^{(1)}$ provided $T_{BB}^{(1)}$ is known, while to solve Eq. (4.9) for $T_{BB}^{(1)}$ we need $f^{(1)}$. However, Eq. (4.9) for $T_{BB}^{(1)}(E)$ requires $f^{(1)}(p,\epsilon=E-\omega)$, where ω is the energy of the spectator pion, while Eq. (4.2) for $f^{(1)}(p,\epsilon)$ requires $T_{BB}^{(1)}(\epsilon)$. To avoid this "self-consistency" we need to approximate the energy dependence of the vertices in the crossed diagram. First, we note that, if we include the factor of Z_2 for the internal baryon propagators, then each vertex appearing in the crossed diagram is fully renormalized, i.e., of the form $Z_2^{1/2}f^{(1)}Z_2^{1/2}$, and therefore should reproduce the experimental coupling constant. Second, for low energy scattering, we are mainly interested in energies $E<m_N+2m_\pi$. This means that the vertices $f^{(1)}(\epsilon)$ needed for the crossed diagram are at any energy $\epsilon=E-\omega_p<m_N+m_\pi$. At these energies, $f^{(1)}$ is a real function, having no contribution to two-body unitarity. It is therefore appropriate to neglect its energy dependence and take the vertices in Eq. (4.6) to be

$$f^{(1)}(p;E)\simeq f_R^{(2)}(p) \ , \qquad (4.10)$$

where the subscript R is to indicate that the coupling constant should be adjusted so that $f_R^{(2)}$ yields the physical coupling constants. Hence in the crossed diagram we use the vertex of Eq. (A2) with $f_{\pi NN}^2=0.08u^2(p_0R)$, which ensures that the physical πNN coupling constant is reproduced. Although the bare πNN, πNΔ, and $\pi\Delta\Delta$ coupling constants are related by the bag model, there is no reason

FIG. 9. The disconnected $\pi\pi$B$\leftrightarrow\pi\pi$B amplitude $M_d^{(2)}$.
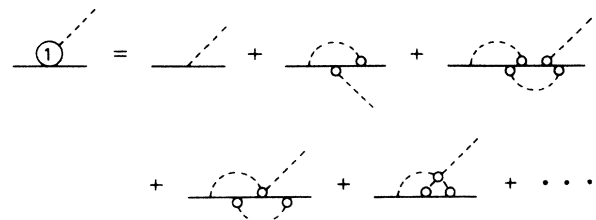

FIG. 10. Diagrammatic equivalent to Eq. (4.8). The small circles represent a one-particle irreducible amplitude.
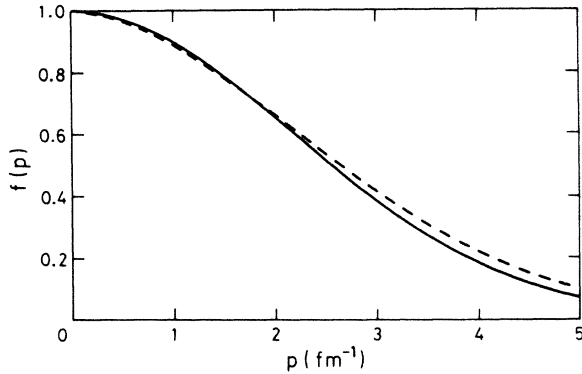
FIG. 11. The bare (solid curve) and renormalized (dashed curve) vertex functions.

to expect that the renormalized coupling constants extracted from $f^{(1)}$ will be in the same ratio. Ideally, if the model works perfectly, the renormalized coupling constants should all reproduce the experimental values. Hence, rather than take the coupling constants in the crossed diagram to be in the bag ratios, we take $f_{\pi NN} : 3f_{\pi N\Delta} = 1:2$, as dictated by experiment.[16] Since experimental guidance as to the value of the $\pi\Delta\Delta$ coupling is unclear, we use the bag model ratio for $f_{\pi NN} : f_{\pi\Delta\Delta}$. The effectiveness of approximating the momentum dependence of the dressed vertex by that of the undressed vertex is illustrated in Fig. 11, where we show the bare vertex function $f(p) = u(pR)$ (solid curve), and the equivalent, appropriately normalized, dressed function $f(p) \sim f_{\pi NN}^{(1)}(p; m_N)/p$ (dashed curve) for a typical case.

For consistency, the pole diagram should include a factor of $Z_2^{1/2}$ on each external leg (but no factor of Z_2 for the internal baryon line). This can be done by using

$$f_0 \equiv Z_{2N}^{1/2} f_{\pi NN} \qquad (4.11)$$

instead of $f_{\pi NN}$ as the coupling constant for the vertex $f^{(2)}$ appearing in Eq. (4.2).

The above discussion means that the only change needed to the equations of Sec. II is use of the experimental coupling constant in vertices contributing to the crossed diagram and f_0 in the vertex $f^{(2)}$ of Eqs. (2.3) and (2.5). Also, Eq. (2.30) becomes

$$f_{\pi NN}^R = f_0 \frac{\tilde{f}_{\pi NN}^{(1)}(p_0, m_N)}{f_{\pi NN}^{(2)}(p_0)} Z_{2N}^{1/2} u(p_0 R) . \qquad (4.12)$$

Since Z_2 depends on f_0 and not on $f_{\pi NN}$ and Z_2 independently, the above prescription avoids the problems of self-consistency in calculating Z_2 alluded to just before Eq. (2.1). We now adjust f_0 to obtain the experimental coupling constant from Eq. (4.12) and use Eq. (4.11) to determine the bare coupling constant $f_{\pi NN}$.

V. THREE-BODY EQUATIONS: RESULTS

Now that we have a model in which we have eliminated the inconsistency between the calculation of the renormalization and the scattering, we can begin to examine its consequences. The first case considered is in the absence
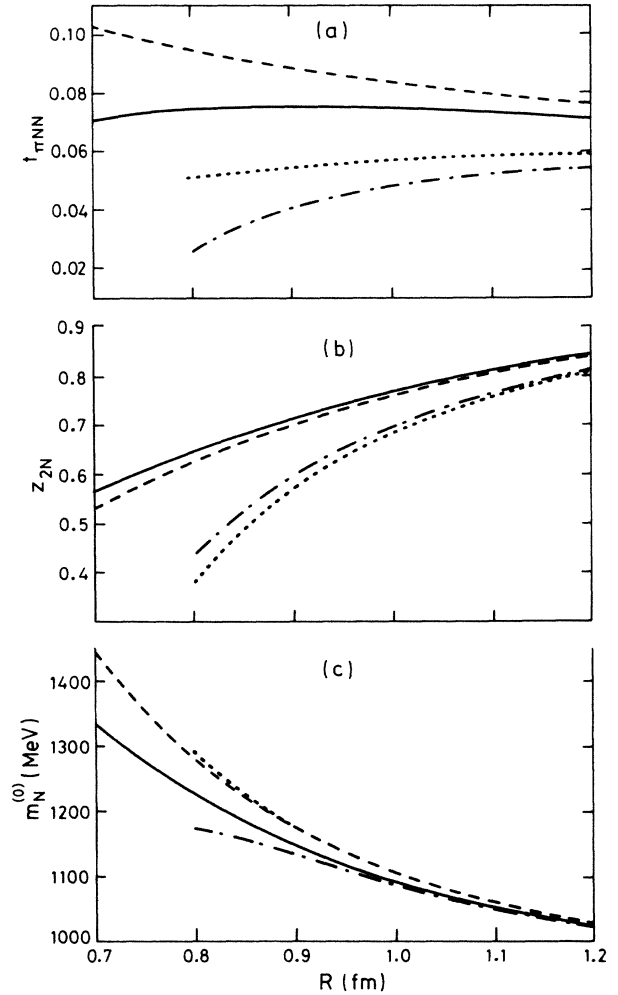

FIG. 12. The bare coupling constant, nucleon wave function renormalization, and bare nucleon mass as functions of the bag radius using the renormalized coupling constant in the crossed diagram. Solid curve is with the crossed diagram as the only contribution to $t^{(2)}$, dashed curve is the same but with crossed diagrams coupling constants in bag ratios, dashed-dotted curve is with crossed and contact diagrams, while the dotted curve is the same but with coupling constants in bag ratios.

of the contact or Roper pole diagrams. In Fig. 12 (solid curve) we show the resulting bare coupling constant $f_{\pi NN}$, Z_{2N}, and the bare nucleon mass for a range of bag radii (the dashed curve shows results obtained when the coupling constants in the crossed diagrams vertices are in the bag [i.e., SU(6)] ratios). The most notable difference between this and the earlier results in Fig. 5 is that the bare coupling constant now remains relatively stable as the radius is reduced. The corresponding P_{11} phase shifts for a radius of 1 fm are shown in the solid curve of Fig. 13. Clearly, some other source of attraction is required to make the phase shifts change sign.

The next step is to include the contact diagram. The renormalization results with the pion decay constant f_π set to the experimental value of 93 MeV in the contact term, are shown in the dashed-dotted curve of Fig. 12 (the dotted curve is with the crossed diagram's coupling con-
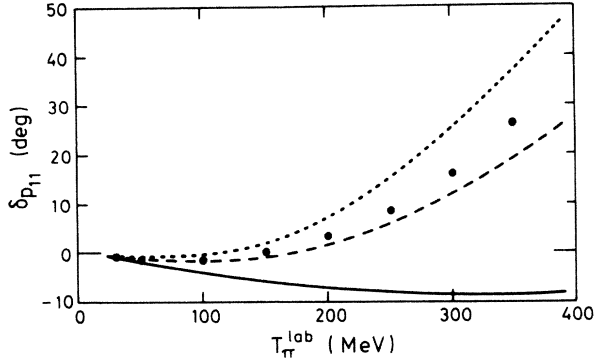
FIG. 13. The P_{11} phase shifts for a bag radius of 1 fm and $f_\pi = 93$ MeV. The solid curve is with only the crossed diagram contributing to $t^{(2)}$, the dashed curve is with crossed and contact diagrams, while the dotted curve is with crossed, contact, and Roper pole diagrams. Experimental data are from Ref. 18.

FIG. 15. P_{11} phase shifts with crossed and contact diagrams. Solid curve is with $f_\pi = 90$ MeV; dashed curve has $f_\pi = 93$ MeV. Experimental data are from Ref. 18.

stants in the bag ratio). In this case the bare coupling constant is significantly lower than was the case without the contact diagram, over a larger range of bag radii. This has the effect of significantly reducing the repulsive nucleon pole diagram which, when combined with the extra attraction of the contact diagram, greatly improves the fit to the P_{11} phase shifts, as can be seen in Fig. 13 (for $R = 1$ fm, dashed curve). In Fig. 14 we compare these phase shifts (solid curve) with those obtained if the coupling constants in the crossed diagram are in the bag ratios (dashed curve). As can be seen, using the physical coupling constants as dictated by our formalism results in a better fit.

It is interesting to see if the fit can be improved by *ad hoc* adjustment of the pion decay constant f_π. It is found that increasing the strength of the contact diagram (which adds needed attraction) also decreases the value of the bare coupling constant and, consequently, the strength of the repulsive nucleon pole diagram. This combined action means that f_π only needs to be reduced from 93 to 90 MeV in order to produce the excellent fit shown in the solid curve of Fig. 15. (The dashed curve is with $f_\pi = 93$
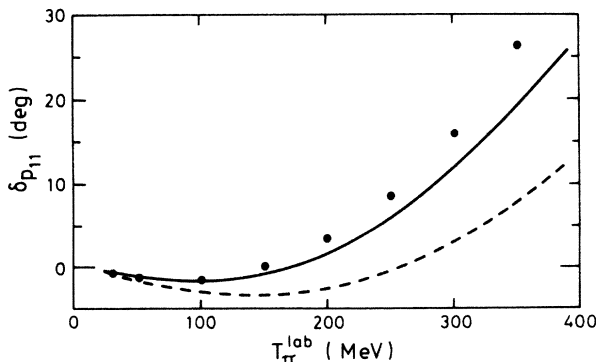
MeV.) In this case, we have $R = 1$ fm, $f_{\pi NN} = 0.0459$, $Z_{2N} = 0.6962$, and $m_N^{(0)} = 1086$ MeV. This fit is quite remarkable in the context of recent investigations of the P_{11} channel (that iterate potentials generated from the CBM in a Lippmann-Schwinger—type equation), which have all required the inclusion of the Roper pole diagram in order to produce enough attraction to cancel the repulsive nucleon pole.[3,5] In these analyses, even though the phase shifts are made to go through 90° at the physical Roper mass, the shape is completely wrong at lower energies. In contrast, our method succeeds by reducing the strength of the nucleon pole rather than trying to cancel it by adding more attraction. The question of whether one should reduce the repulsion or increase the attraction is important in the πNN system, where the pole and nonpole parts of the P_{11} amplitude enter into the calculation in differing ways.[17] In view of this, in Fig. 16 we show the phase shifts from the nonpole part of the amplitude, $T_{BB}^{(1)}$ (dashed curve), as well as from the full amplitude (solid curve) for the case of $R = 1$ fm and $f_\pi = 90$ MeV described above. We note here that $T_{BB}^{(1)}$ gives rise to a resonance without the explicit introduction of the Roper

FIG. 14. P_{11} phase shifts with crossed and contact diagrams and $f_\pi = 93$ MeV. Solid curve is with physical coupling constants in the crossed diagram; dashed curve is with coupling constants in bag ratio. Experimental data are from Ref. 18.
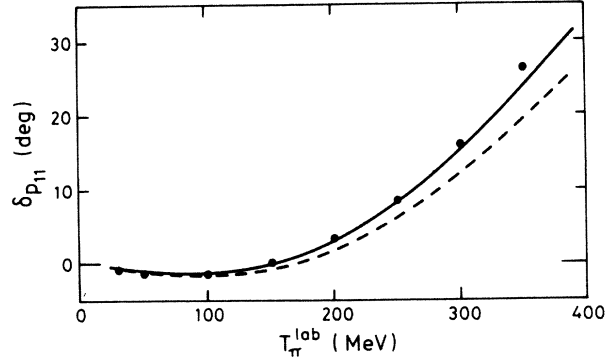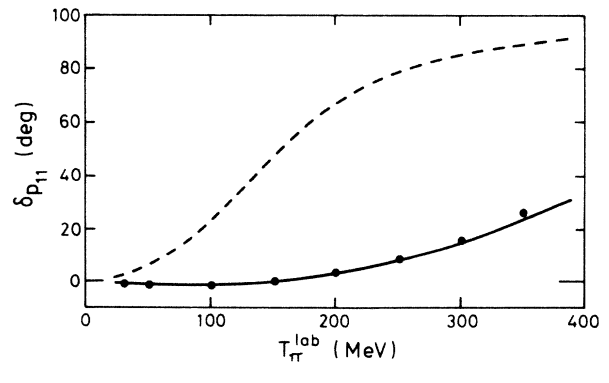

FIG. 16. The total (solid curve) and nonpole (dashed curve) P_{11} phase shifts for $R = 1$ fm, $f_\pi = 90$ MeV, crossed and contact diagrams contributing to $t^{(2)}$. Experimental data are from Ref. 18.
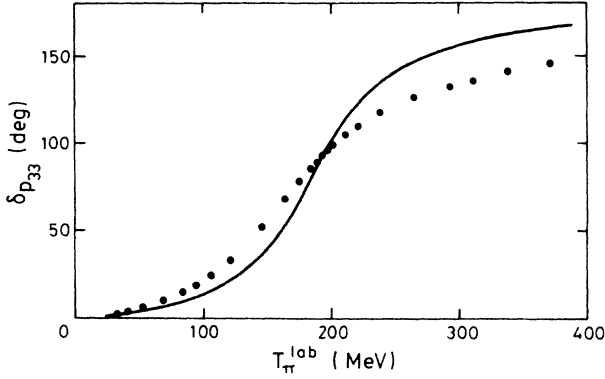
FIG. 17. The P_{33} phase shifts corresponding to the dashed-dotted curve in Fig. 12. Experimental data are from Ref. 19.

FIG. 19. P_{13} phase shifts for $R=1$ fm, $f_\pi=90$ MeV. Experimental data are from Ref. 19.

in terms of bag states $[(1s_{1/2})^2 2s_{1/2}]$. The addition of the pole amplitude has the effect of shifting the resonance to higher energy.

Despite the success obtained without the Roper pole, it is interesting to examine the effect of including it. As usual, with f_π set to 93 MeV we adjust the bare coupling constant to obtain the correct renormalized coupling constant, while the bare Roper mass is adjusted to make the phase shifts go through 90° at the correct energy. For $R=1$ fm we find $f_{\pi NN}=0.0418$, $Z_{2N}=0.7112$, $m_N^{(0)}=1076$ MeV, and $m_R^{(0)}=1640$ MeV, with the P_{11} phase shifts shown in the dotted curve of Fig. 13. The poor fit in this case is an indication that one should not adjust the Roper bare mass to get the phase shifts through 90° without simultaneously satisfying three-body unitarity.

Unfortunately, it would appear that the price to be paid for the improvement in the P_{11} phase shifts is a reduction in the quality of the fit in the P_{33} channel. Using the parameters that gave the best fit to the P_{11} channel (i.e., $R=1$ fm, $f_\pi=90$ MeV) results in the fit shown in Fig. 17. In this calculation the bare delta mass is adjusted so that the phase shifts pass through 90° at the delta mass. The fact that the width is so small is an indication that the amount of renormalization of $f_{\pi N\Delta}$ is insufficient. This is best illustrated by calculating the quantity η_r of
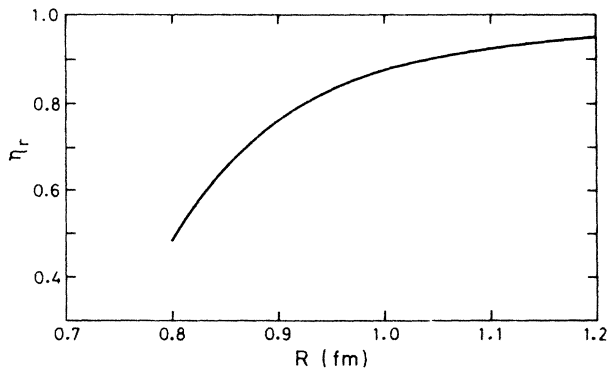
Ref. 2, which is a comparison of the degree of renormalization of the πNN and $\pi N\Delta$ coupling constants. In our notation this is

$$\eta_r = \left[\frac{f_{\pi N\Delta}^R}{f_{\pi N\Delta}} \frac{f_{\pi NN}}{f_{\pi NN}^R} \right]^2 = \left[\frac{g_{NN} f_{\pi N\Delta}^R}{g_{N\Delta} f_{\pi NN}^R} \right]^2 , \quad (5.1)$$

where the matrix g is given in Eq. (A5). Analogously to Eq. (4.12), the renormalized $\pi N\Delta$ coupling constant is given by

$$f_{\pi N\Delta}^R = \frac{f_0 g_{N\Delta}}{g_{NN}} \frac{f_{\pi N\Delta}^{(1)}(p_0, m_N)}{f_{\pi N\Delta}^{(2)}(p_0)} Z_{2\Delta}^{1/2} u(p_0 R) , \quad (5.2)$$

and $Z_{2\Delta}$ is taken to be

$$Z_{2\Delta} = \left[1 - \frac{\partial}{\partial E} \Sigma_{\Delta\Delta}^{(1)}(E = m_N) \right]^{-1} . \quad (5.3)$$

The quantity η_r as a function of bag radius is shown in Fig. 18 for the case of no Roper pole and $f_\pi=93$ MeV. This shows that the renormalization of $f_{\pi N\Delta}$ is less than that of $f_{\pi NN}$, in contradiction with the physical value of[16] $\eta_r \approx 1.5$.

The final application we wish to consider is the P_{13} and P_{31} partial waves. These are independent of the bare cou-

FIG. 18. Ratio of renormalization of $f_{\pi N\Delta}$ and $f_{\pi NN}$, η_r.
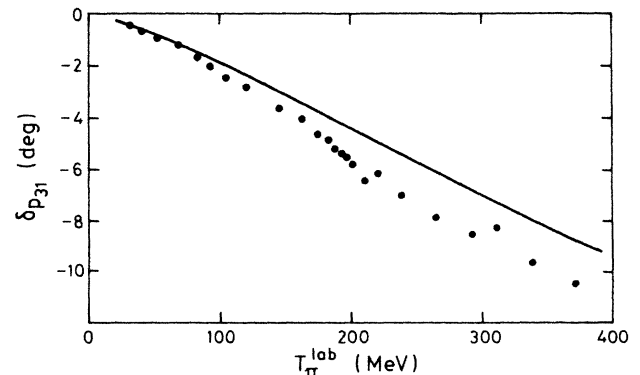

FIG. 20. P_{31} phase shifts as for Fig. 19. Experimental data are from Ref. 19.

pling constant, having contributions only from the crossed and contact diagrams. Using the parameters giving the best P_{11} fit, namely $R = 1$ fm and $f_\pi = 90$ MeV, we obtain the results illustrated in Figs. 19 and 20.

VI. CONCLUSIONS

We have examined the implications of calculating the renormalization of the CBM πNN coupling constant using the same series of diagrams that arise in a Lippmann-Schwinger—type calculation of the phase shifts. We find a large discrepancy between this approach and that which is obtained by using only those diagrams to second order in the bare coupling constant. This discrepancy can be attributed to the omission of a certain class of diagrams from the Lippmann-Schwinger equation which are important in the renormalization due to cancellation. These diagrams are included in a description of the πN system that respects two- and three-body unitarity by correctly incorporating two-pion states. At energies below the two-pion threshold, these equations can be approximated in a way that provides greater insight into how the crossed diagram should be treated in the two-body Lippmann-Schwinger equation. In particular, the πBB vertices that

form the crossed diagram should have the physical rather than bare coupling constant, since the two-body Lippmann-Schwinger equation does not contribute to the dressing of these vertices as it includes two-body unitarity only. On the other hand, the vertices in the pole diagram are dressed when the Lippmann-Schwinger equation is solved. When this is put into effect, the bare coupling constant required to reproduce the experimental value is significantly less than previously. As a result, the repulsion in the P_{11} channel is reduced enabling immense improvement in the fit to the phase shifts without necessitating the introduction of extra attraction.

APPENDIX

We use the version of the CBM in which the pion couples to the quarks throughout the bag volume.[8] The Lagrangian expanded to second order in the pion field is

$$\mathcal{L} = \left[\frac{i}{2}\bar{q}(x)\gamma^\mu \overleftrightarrow{\partial}_\mu q(x) - B \right]\theta_V - \frac{1}{2}\bar{q}(x)q(x)\Delta_S + \frac{1}{2}(\partial_\mu\phi)^2 + \frac{1}{2f_\pi}\bar{q}(x)\gamma^\mu\gamma_5\tau\cdot\partial_\mu\phi q(x)\theta_V - \frac{1}{4f_\pi^2}\bar{q}(x)\gamma^\mu\tau\cdot(\phi\times\partial_\mu\phi)q(x)\theta_V ,$$

(A1)

where $q(x)$ and $\phi(x)$ are the quark and pion fields, f_π is the pion decay constant, and B is the bag energy density. Δ_S is a surface delta function and θ_V is 1 inside and 0 outside the bag. After projection onto the subspace of baryons consisting of the nucleon, delta, and Roper [assuming the Roper to be a $(1s_{1/2})^2(2s_{1/2})$ configuration] in the usual way, the interaction part of this Lagrangian yields a B$\leftrightarrow\pi$B vertex, a πB$\leftrightarrow\pi$B contact term, as well as a B$\leftrightarrow\pi\pi$B vertex. In the present work we neglect the

B$\leftrightarrow\pi\pi$B vertex, taking the remaining two terms as the driving terms for our description of the πN system. The formulas we present here are after partial wave expansion, suitable for use in the partial-wave expanded equations presented in the main text.

The basic vertex function is

$$f^{(2)}_{\pi\alpha\beta}(p) = \frac{4\pi i}{(2\pi)^{3/2}\sqrt{2\omega_p}}\frac{f_{\pi NN}}{m_\pi}pg_{\alpha\beta}G_{\alpha\beta}(p) ,$$

(A2)

with

$$G_{\alpha\beta}(p) = u(pR) - \left[\frac{\omega_\alpha}{R} - \frac{\omega_\beta}{R} + \omega_p\right]\frac{3}{2R^3 j_0(\omega_\alpha)j_0(\omega_\beta)}\int_0^R dr\, r^2 \frac{j_1(pr)}{p}\left[j_0\left[\frac{\omega_\alpha r}{R}\right]j_1\left[\frac{\omega_\beta r}{R}\right] - j_1\left[\frac{\omega_\alpha r}{R}\right]j_0\left[\frac{\omega_\beta r}{R}\right]\right] ,$$

(A3)

$$u(pR) = \frac{3j_1(pR)}{pR} ,$$

(A4)

and the matrix of coefficients $g_{\alpha\beta}$ given by

$$g = \frac{\sqrt{3}}{5}\begin{bmatrix} 5 & 2\sqrt{2} & 5\phi \\ 4\sqrt{2} & 5 & 4\sqrt{2}\phi \\ 5\phi & 2\sqrt{2}\phi & 5\phi^2 \end{bmatrix}, \quad \phi = \left[\frac{\omega_2(\omega_1-1)}{3\omega_1(\omega_2-1)}\right]^{1/2} .$$

(A5)

Here, ω_1 and ω_2 are 2.04 and 5.40, respectively, and

$\omega_\alpha = \omega_1$ if $\alpha = $ N,Δ and $\omega_\alpha = \omega_2$ if $\alpha = $ R. ω_p is the energy of the pion. The first term of Eq. (A3) is the same as arises in the surface-coupling form of the CBM, while the second term only contributes to vertices that involve a $1s\leftrightarrow2s$ quark transition.

From this vertex and the baryon propagator, we can construct the crossed diagram which will contribute to the potential $t^{(2)}$, giving

$$t_{\alpha\beta}^{(2)IJT\,\text{cross}}(p,p';E)=\sum_{\gamma L}f_{\pi\gamma\beta}^{(2)}(p)d_{\gamma}^{L}(p,p';E)f_{\alpha\gamma\pi}^{(2)}(p')A_{\alpha\beta\gamma L}^{IJT}\ ,\tag{A6}$$

with

$$d_{\gamma}^{L}(p,p';E)=2\pi\int_{-1}^{1}\frac{P_{L}(x)dx}{E-(p^{2}+p'^{2}+2pp'x+m_{\gamma}^{2})^{1/2}-\omega_{p}-\omega_{p'}}\ ,\tag{A7}$$

where P_{L} is the Legendre polynomial of order L, and

$$A_{\alpha\beta\gamma L}^{IJT}=\frac{3}{4\pi}\hat{L}^{2}\hat{l}^{2}\hat{s}_{\alpha}\hat{s}_{\beta}\hat{\tau}_{\alpha}\hat{\tau}_{\beta}(-1)^{2l+\tau_{\alpha}+\tau_{\beta}}\begin{pmatrix}1 & L & l\\0 & 0 & 0\end{pmatrix}^{2}\begin{Bmatrix}\tau_{\beta} & 1 & T\\\tau_{\alpha} & 1 & \tau_{\gamma}\end{Bmatrix}\begin{Bmatrix}l & J & s_{\beta}\\1 & s_{\alpha} & s_{\gamma}\\L & l & 1\end{Bmatrix}\ ,\tag{A8}$$

where $\hat{j}=(2j+1)^{1/2}$, and s_{α} and τ_{α} are the spin and isospin of baryon α, respectively.

The contact diagram, which also contributes to $t^{(2)}$, consists of three parts, the first arising from the time derivatives in the Lagrangian and the second two from the spatial derivatives.

$$t_{\alpha\beta}^{(2)IJT\,\text{contact}}(p,p')=\frac{1}{f_{\pi}^{2}(2\pi)^{3}\sqrt{2\omega_{p}2\omega_{p'}}}[_{T}u_{\alpha\beta}^{l}(p,p')C_{\alpha\beta}^{JT}+_{S1}u_{\alpha\beta}^{l}(p,p')C_{\alpha\beta}^{JT}+_{S2}u_{\alpha\beta}^{l}(p,p')B_{\alpha\beta}^{IJT}]\ ,\tag{A9}$$

where

$$_{T}u_{\alpha\beta}^{l}(p,p')=(\omega_{p}+\omega_{p'})\int_{0}^{R}dr\,r^{2}\left[j_{0}\left[\frac{\omega_{\alpha}r}{R}\right]j_{0}\left[\frac{\omega_{\beta}r}{R}\right]+j_{1}\left[\frac{\omega_{\alpha}r}{R}\right]j_{1}\left[\frac{\omega_{\beta}r}{R}\right]\right]j_{l}(pr)j_{l}(p'r)\ ,\tag{A10}$$

$$_{S1}u_{\alpha\beta}^{l}(p,p')=\int_{0}^{R}dr\,r^{2}\left[j_{0}\left[\frac{\omega_{\alpha}r}{R}\right]j_{1}\left[\frac{\omega_{\beta}r}{R}\right]-j_{1}\left[\frac{\omega_{\alpha}r}{R}\right]j_{0}\left[\frac{\omega_{\beta}r}{R}\right]\right][p'j_{l}(pr)j_{l+1}(p'r)-pj_{l+1}(pr)j_{l}(p'r)]\ ,\tag{A11}$$

and

$$_{S2}u_{\alpha\beta}^{l}(p,p')=\int_{0}^{R}dr\,r\left[j_{0}\left[\frac{\omega_{\alpha}r}{R}\right]j_{1}\left[\frac{\omega_{\beta}r}{R}\right]+j_{1}\left[\frac{\omega_{\alpha}r}{R}\right]j_{0}\left[\frac{\omega_{\beta}r}{R}\right]\right]j_{l}(pr)j_{l}(p'r)\ ,\tag{A12}$$

and the coefficients B and C are

$$B_{\alpha\beta}^{IJT}=2\pi\sqrt{6}N_{\alpha}N_{\beta}g_{\alpha\beta}'(-1)^{s_{\alpha}-s_{\beta}+J+\tau_{\alpha}-\tau_{\beta}+T+l+1}\hat{l}\sqrt{l(l+1)}\begin{Bmatrix}l & s_{\beta} & J\\s_{\alpha} & l & 1\end{Bmatrix}\begin{Bmatrix}1 & \tau_{\beta} & T\\\tau_{\alpha} & 1 & 1\end{Bmatrix}\tag{A13}$$

and

$$C_{\alpha\beta}^{JT}=\pi\sqrt{6}N_{\alpha}N_{\beta}g_{\alpha\beta}''(-1)^{3/2+\tau_{\alpha}-\tau_{\beta}+T}\begin{Bmatrix}1 & 1 & 1\\\tau_{\alpha} & T & \tau_{\beta}\end{Bmatrix}\ .\tag{A14}$$

The coefficient matrices g' and g'' are given by

$$g'=\begin{bmatrix}10 & 8\sqrt{2} & \dfrac{10}{\sqrt{3}}\\8\sqrt{2} & 20 & 8\dfrac{\sqrt{2}}{\sqrt{3}}\\\dfrac{10}{\sqrt{3}} & 8\dfrac{\sqrt{2}}{\sqrt{3}} & \dfrac{10}{3}\end{bmatrix},\quad g''=\begin{bmatrix}\sqrt{6} & 0 & \sqrt{2}\\0 & -2\sqrt{15} & 0\\\sqrt{2} & 0 & \dfrac{\sqrt{2}}{\sqrt{3}}\end{bmatrix},\tag{A15}$$

and the normalization coefficient is

$$N_{\alpha}=\left[\frac{\omega_{\alpha}}{2(\omega_{\alpha}-1)}\right]^{1/2}\frac{1}{R^{3/2}j_{0}(\omega_{\alpha})}\ .\tag{A16}$$

[1]S. Theberge, A. W. Thomas, and G. A. Miller, Phys. Rev. D 22, 2838 (1980); 23, 2106(E) (1981); A. W. Thomas, S. Theberge, and G. A. Miller, *ibid*. 24, 216 (1981); A. W. Thomas, Adv. Nucl. Phys. 13, 1 (1984).

[2]S. Theberge, G. A. Miller, and A. W. Thomas, Can. J. Phys. 60, 59 (1982).

[3]E. A. Veit, B. K. Jennings, and A. W. Thomas, Phys. Rev. D 33, 1859 (1986).

[4]E. A. Veit, A. W. Thomas, and B. K. Jennings, Phys. Rev. D 31, 2242 (1985).

[5]A. S. Rinat, Nucl. Phys. A377, 341 (1982).

[6]B. Blankleider and G. E. Walker, Phys. Lett. 152B, 291 (1985).

[7]J. A. Johnstone and T.-S.H. Lee, Argonne Report No. PHY-4666-TH-85, 1985 (unpublished).

[8]A. W. Thomas, J. Phys. G 7, L283 (1981); A. Szymacha and S. Tatur, Z. Phys. C 7, 311 (1981).

[9]I. R. Afnan and B. C. Pearce, submitted to Phys. Rev. C.

[10]I. R. Afnan and A. T. Stelbovics, Phys. Rev. C 23, 1384 (1981).

[11]T. Mizutani, C. Fayard, G. H. Lamot, and S. Nahabetian, Phys. Rev. C 24, 2633 (1981).

[12]We say an amplitude is n-particle irreducible if no diagrams that contribute to that amplitude can be split in two by a line separating initial and final states that cuts k particle lines (at least one of which must be internal), for any $k \le n$. For further details, see Ref. 13.

[13]I. R. Afnan and B. Blankleider, Phys. Rev. C 32, 2006 (1985).

[14]S. Morioka and I. R. Afnan, Phys. Rev. C 26, 1148 (1982).

[15]M. G. Fuda, Phys. Rev. C 32, 2024 (1985).

[16]M. M. Nagels *et al.*, Nucl. Phys. B147, 189 (1979).

[17]I. R. Afnan and R. J. McLeod, Phys. Rev. C 31, 1821 (1985).

[18]R. A. Arndt, J. M. Ford, and L. D. Roper, Phys. Rev. D 32, 1085 (1985).

[19]R. Koch and E. Pietarinen, Nucl. Phys. A336, 331 (1980).